

Dissociative recombination of $e + \text{HCNH}^+$: Diabatic potential curves and dynamics calculations

A. P. Hickman¹, R. D. Miles¹, C. Hayden¹, and D. Talbi²

¹ Department of Physics, Lehigh University, 16 Memorial Dr. East, Bethlehem, PA, 18015, USA
e-mail: aph2@lehigh.edu

² LETMEX, Muséum National d'Histoire Naturelle, 57 rue Cuvier, Case Postale 52, 75231 Paris Cedex 05, France
e-mail: talbi@mnhn.fr

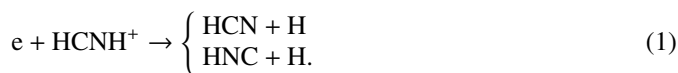
Received 7 January 2005 / Accepted 13 April 2005

Abstract. Adiabatic and diabatic potential curves are obtained for linear HCNH. The electronic states of this molecule are characterized by strong mixing of valence and Rydberg configurations. Molecular orbitals for these two classes of configurations are determined separately and then combined. Large scale calculations at the level of single and double excitations from a multi-configuration reference are performed. The calculations confirm the earlier results of Talbi & Ellinger (1998, *Chem. Phys. Lett.*, 288, 155). Diabatic potential curves are determined using the block diagonalization method and are used to estimate the width Γ for electron capture by HCNH^+ . Rates for dissociative recombination through the CH bond and through the NH bond (which lead to $\text{HNC} + \text{H}$ and $\text{HCN} + \text{H}$, respectively) are calculated using a simple quasi-diatomic model. None of the calculated results suggests a strong difference in the rates for production of HNC and HCN.

Key words. molecular processes – ISM: abundances

1. Introduction

There has been much interest recently in the branching ratio of the dissociative recombination (DR) process



This process is important in the interstellar medium. Indeed, among the puzzles still unresolved in astrochemistry is the explanation for the variation of the HNC/HCN abundance ratios observed in different locations in space. In dark cold clouds (TMC-1) HNC/HCN is 1.55 (Irvine & Schloerb 1984). In OMC-1, a region of high mass star formation, this same abundance ratio changes drastically from 1/80 in the immediate vicinity of Orion-KL to values in the range of 1/5 for adjacent ridge positions (Schilke et al. 1992). In order to reproduce the abundances observed for HCN and HNC, astrochemical models have hypothesized that the dissociative recombination of HCNH^+ leads to an equal amount of HCN and HNC.

There have been several recent calculations of potential curves for this system (Talbi & Ellinger 1998; Shiba et al. 1998; Semaniak et al. 2001), and several groups have discussed the dynamics of the process (Tachikawa 1999; Semaniak et al. 2001). Talbi & Ellinger (1998) performed a quantum chemical ab initio study using a quasi-diabatic representation. They found that the two lowest $\text{HCNH}^+ \ ^2\Sigma$ dissociative states, which lead to HCN and HNC fragments, respectively, cross the potential energy surface of the HCNH^+ ion near its minimum and

below the first vibrational level. They also found that each of these dissociative states crosses the lowest series of HCNH Rydberg states, but above the minima and between the first and second vibrational levels. On the basis of these crossings Talbi and Ellinger have suggested that if the total DR of HCNH^+ (including both the direct and the indirect mechanism) leads to equal amounts of HCN and HNC, the direct process would be more efficient than the indirect.

The diabatic potential energy curves calculated by Shiba et al. (1998) lead to a different conclusion. Shiba et al. (1998) found that the two lowest $\text{HCNH}^+ \ ^2\Sigma$ dissociative states (leading to HCN and HNC) do not cross the potential energy curve of the ion. However, they did not include Rydberg orbitals in their atomic basis set. Rydberg orbitals are crucial to describe the two lowest $\ ^2\Sigma$ valence dissociative states of HCNH. Indeed, from their analysis of the CI adiabatic wave functions, Talbi & Ellinger (1998) showed that at the ion equilibrium geometry the two lowest $\ ^2\Sigma$ states of HCNH are of Rydberg character and change to dissociative character as the CH or NH bond is stretched, leading respectively to HNC or HCN. Such a change in character from Rydberg to valence dissociative cannot appear in the calculations of Shiba et al. due to the lack of Rydberg basis functions. The neglect of Rydberg orbitals might explain why the diabatic dissociative states of Shiba et al. pass below the ionic curve of HCNH rather than crossing it.

The theoretical and experimental study undertaken by Semaniak et al. (2001) aimed at exploring CN formation

from the dissociative recombination of HCNH⁺ confirmed the easy formation of HCN and HNC from this process. Finally, Tachikawa (1999) has shown by means of direct ab initio dynamics calculations that at low temperature the direct processes dominates in the DR of HCNH⁺ even though he suggests for the low temperature of the interstellar medium the dominant formation of HNC.

Because of the differences among the studies described above, many issues regarding the DR of HCNH⁺ are not yet settled. In the present study, we report a calculation of diabatic potential curves for linear HCNH using the block diagonalization method (Pacher et al. 1988), and we use these curves and coupling terms to estimate cross sections for the direct DR process. Implementing the block diagonalization method required a new set of electronic structure calculations, which also confirmed the earlier calculations of Talbi & Ellinger (1998) of the adiabatic potential curves.

2. Potential curves

This section describes the ab initio electronic structure calculations that we performed to determine adiabatic and diabatic potential curves. We first summarize briefly the block diagonalization method used to determine diabatic curves, since implementing this method requires a few extra steps in the procedure.

2.1. Block diagonalization method

The block diagonalization method (Pacher et al. 1988) provides an effective technique for transforming the results of a standard electronic structure calculation into diabatic potential curves. An advantage of the method is that one can perform a conventional calculation of the desired size and accuracy and then obtain diabatic curves with comparable reliability. A second advantage is that the numerical effort for the diabatization is quite modest compared to the original calculation (which usually involves diagonalizing a very large, sparse matrix).

The method requires extra effort in the determination of molecular orbitals (mo's). Briefly, one must insure that the variation of the mo's $\{\phi_i\}$ with molecular geometry is small. This result can be achieved by setting up the calculation in such a way that the adiabatic energies are invariant under a rotation of certain molecular orbitals, and then selecting an appropriate rotation at each geometry. For example, the MCSCF energies are invariant under an arbitrary rotation \mathbf{U} of the mo's in the active space (Roos 1987; Schmidt & Gordon 1998). One can replace a set of orbitals ϕ'_i optimized in an MCSCF with a new set

$$\phi_i = \sum_j U_{ij} \phi'_j, \quad (2)$$

and the MCSCF energies will not change. Pacher et al. (1988) pointed out that one can take advantage of this degree of freedom by choosing U so that each mo in the set $\{\phi_i\}$ resembles as closely as possible a corresponding orbital in a set of "reference" orbitals. The reference orbitals are defined in a way that makes them easy to interpret and ensures that they are slowly varying. We use the algorithm we previously implemented (Spirko et al. 2000) based on a series of Jacobi rotations

to maximize the overlap of each ϕ_i with the corresponding reference orbital.

The configuration interaction (CI) electronic wave function Ψ_n for the n th state is represented as the sum of configurations Φ_m , each constructed from the mo's ϕ_i :

$$\Psi_n = \sum_{m=1}^N c_{mn} \Phi_m. \quad (3)$$

The number of coefficients N in the sum in Eq. (3) may be quite large (of order 10^6). However, one can usually identify a small set of N_α configurations ($N_\alpha \sim 2-10$) that make the dominant contribution to N_α electronic states of interest. Then N_α will be the dimension of the diabatic Hamiltonian, and for the diabatization one only needs the $N_\alpha \times N_\alpha$ matrix of values c_{mn} for the coefficients of the N_α dominant configurations in the N_α states of interest. We denote this matrix by \mathbf{S} . The diabatic Hamiltonian matrix $\mathbf{H}_{\text{diabatic}}$ can be expressed as a transformation of the diagonal matrix \mathbf{E} whose nonzero elements are the adiabatic eigenvalues E_1, \dots, E_{N_α} :

$$\mathbf{H}_{\text{diabatic}} = \mathbf{T}^\dagger \mathbf{E} \mathbf{T}, \quad (4)$$

where $(^\dagger)$ denotes the adjoint (transpose for a real transformation), and

$$\mathbf{T} = \mathbf{S}^{-1} (\mathbf{S} \mathbf{S}^\dagger)^{1/2}. \quad (5)$$

This analysis of the adiabatic eigenvalues and eigenvectors is straightforward and only involves matrices of order N_α . Since $\mathbf{H}_{\text{diabatic}}$ is explicitly constructed by a unitary transformation of the matrix \mathbf{E} of adiabatic eigenvalues, the eigenvalues of the small matrix $\mathbf{H}_{\text{diabatic}}$ will be exactly the same as the chosen N_α eigenvalues of the large matrix determined by the CI calculation.

2.2. Electronic structure calculations

These calculations were performed with the GAMESS code (Schmidt et al. 1993). We used the Dunning-Hay double zeta basis set (Dunning & Hay 1977), augmented with an additional polarization function on each H, one additional diffuse sp and one polarization function (six cartesian d functions) on C and N, and two additional Rydberg s and p functions on the midpoint of CN. The total number of basis functions was 56. The exponents of the Rydberg functions were 0.026 and 0.016 for the s functions and 0.023 and 0.015 for the p functions. The Rydberg exponents are the same as those previously used by Talbi & Ellinger (1998).

Talbi & Ellinger (1998) originally discussed the special requirements for an electronic structure calculation of dissociating potential curves for linear HCNH. It is important to treat both the CH bond and the NH bond equally and in a manner that correctly describes the dissociation process. The valence space must therefore include both bonding and antibonding orbitals for the CH and the NH bonds. It is also important to include diffuse Rydberg orbitals. The coupling between configurations involving these types of orbitals controls the electron capture process, and the calculated adiabatic wave functions exhibit considerable mixing of these types of configurations.

Table 1. Equilibrium geometry for HCNH⁺.

R_{CH}	R_{CN}	R_{NH}
1.916 a_0	2.141 a_0	2.041 a_0

The calculations we performed were designed to probe the dependence of the potential surface on the CH or NH coordinate. For all calculations, we froze the parameters of the bonds not being stretched at their equilibrium positions. These equilibrium bond distances are given in Table 1. Talbi et al. (1988) found that optimizing the other bond lengths did not significantly change the shape of the potential energy curves with respect to the bond of interest.

Near the linear equilibrium geometry, the orbital occupancy of HCNH⁺ is

$$\dots (\sigma_{\text{CN}})^2 (\sigma_{\text{CH}})^2 (\sigma_{\text{NH}})^2 (\pi_{\text{CN}})^4, \quad (6)$$

where “...” signifies the core 1s orbitals for C and N. The direct mechanism for DR involves capture of an electron incident on this molecular ion into a dissociating state of the corresponding neutral (Bardsley 1968; Giusti 1980; Giusti-Suzor et al. 1983; Hickman 1987). Talbi & Ellinger (1998) identified the HCNH orbitals involved as σ_{CH}^* and σ_{NH}^* . These orbitals correspond to antibonding orbitals localized on CH and NH, respectively. There are two possible dissociating excited states of HCNH, which are described by the orbital occupancies:

$$\dots (\sigma_{\text{CN}})^2 (\sigma_{\text{CH}})^2 (\sigma_{\text{NH}})^2 (\pi_{\text{CN}})^4 (\sigma_{\text{CH}}^*)^1 \quad (7)$$

and

$$\dots (\sigma_{\text{CN}})^2 (\sigma_{\text{CH}})^2 (\sigma_{\text{NH}})^2 (\pi_{\text{CN}})^4 (\sigma_{\text{NH}}^*)^1. \quad (8)$$

Occupancy (7) leads to dissociation along the CH coordinate R_{CH} . As $R_{\text{CH}} \rightarrow \infty$, the bonding orbital σ_{CH} and antibonding orbital σ_{CH}^* smoothly change into a p_z orbital on C and a 1s orbital on H. Similar behavior occurs in occupancy (8) for σ_{NH} and σ_{NH}^* as $R_{\text{NH}} \rightarrow \infty$. This smooth and chemically sensible behavior is exactly what is desired for the orbitals that will describe the diabatic states that describe dissociation to HNC + H or to HCN + H.

We first describe the method we used to determine “reference” orbitals that exhibit this desired behavior. The method is similar to the approach used by Talbi & Ellinger (1998). We performed an MCSCF calculation for the $^5\Sigma$ state of HCNH⁺ at the equilibrium geometry of HCNH⁺ ($^1\Sigma$). The orbital occupancy of this state is

$$\dots (\sigma_{\text{CN}})^2 (\pi_{\text{CN}})^4 (\sigma_{\text{CH}})^1 (\sigma_{\text{NH}})^1 (\sigma_{\text{NH}}^*)^1 (\sigma_{\text{CH}}^*)^1, \quad (9)$$

and we took

$$\sigma_{\text{CH}}, \sigma_{\text{NH}}, \sigma_{\text{NH}}^*, \sigma_{\text{CH}}^*$$

as the active space. We then applied the method of Edmiston & Ruedenberg (1963) to localize the orbitals. This procedure involves finding an appropriate orbital rotation of the form Eq. (2) and is available as an option in GAMESS

Table 2. Numbering convention used for the molecular orbitals.

Number	Orbital	Number	Orbital
1	1 s_{N}	8	σ_{NH}^*
2	1 s_{C}	9	σ_{CH}^*
3	σ_{CN}	10	σ_{Ryd}
4	$\pi_{\text{CN}}(x)$	11	σ_{Ryd}
5	$\pi_{\text{CN}}(y)$	12	$\pi_{\text{CN}}^*(x)$
6	σ_{CH}	13	$\pi_{\text{CN}}^*(y)$
7	σ_{NH}		

(Schmidt et al. 1993). Examination of the rotated orbitals confirmed that near the equilibrium geometry, the orbitals were localized on the CH or NH bonds and clearly exhibited bonding and antibonding character. Following Pacher et al. (1988), we defined the reference orbitals at other geometries using the same set of mo coefficients. These coefficients lead to “shifted mo’s” that are no longer orthogonal, so they must be symmetrically orthogonalized (Szabo & Ostlund 1982). This procedure has been shown (Carlson & Keller 1957) to produce the set of orthonormal mo’s closest to the original set. This method produced the desired mo’s for geometries near the ion’s equilibrium, but in the limits $R_{\text{CH}} \rightarrow \infty$ or $R_{\text{NH}} \rightarrow \infty$, the dissociating orbital did not correctly approach the limit of an isolated hydrogen 1s. We were able to obtain the correct asymptotic behavior by adding another step to the method. We used the symmetrically orthogonalized mo’s as the initial guess for another MCSCF calculation of the $^5\Sigma$ state of HCNH⁺ at the new geometry, and then we applied the method of Edmiston & Ruedenberg (1963) to localize just orbitals σ_{NH}^* and σ_{CH}^* . This method reduces exactly to the our original procedure near the equilibrium and also produced the correct behavior asymptotically.

The fact that Rydberg and valence configurations may mix very strongly in the wave functions of HCNH excited states led us to develop a systematic procedure for obtaining optimized valence and Rydberg mo’s separately. The valence orbitals were determined from a series of calculations on the $^1\Sigma$ ground state of HCNH⁺. We first performed an MCSCF using a large active space,

$$\pi_{\text{CN}}, \sigma_{\text{CH}}, \sigma_{\text{NH}}, \sigma_{\text{NH}}^*, \sigma_{\text{CH}}^*, \pi_{\text{CN}}^*.$$

This MCSCF wave function correctly describes dissociation along either the CH or the NH bond. Then we performed a CI using all single and double excitations from this active space. The number of CSF’s was 710 748. We used the natural orbitals from this calculation to construct the valence orbitals for HCNH. First, we reordered the natural orbitals to correspond to the numbering convention given in Table 2, and we also rotated the four sigma orbitals corresponding to σ_{CH} , σ_{NH} , σ_{NH}^* , and σ_{CH}^* so that they matched the reference orbitals as closely as possible, using the method described earlier (Spirko et al. 2000).

A second MCSCF calculation was performed to determine Rydberg orbitals for the HCNH. The Rydberg configurations of ${}^2\Sigma$ HCNH have the orbital occupancy

$$\cdots (\sigma_{\text{CN}})^2 (\sigma_{\text{CH}})^2 (\sigma_{\text{NH}})^2 (\pi_{\text{CN}})^4 (\sigma_{\text{Ryd}})^1, \quad (10)$$

where σ_{Ryd} is a large, diffuse Rydberg orbital centered on CN. To calculate these orbitals we consider the first two ${}^6\Sigma$ states of HCNH, which have orbital occupancies of the form

$$\cdots (\sigma_{\text{CN}})^2 (\pi_{\text{CN}})^4 (\sigma_{\text{CH}})^1 (\sigma_{\text{NH}})^1 (\sigma_{\text{NH}}^*)^1 (\sigma_{\text{CH}}^*)^1 (\sigma_{\text{Ryd}})^1.$$

We performed an MCSCF calculation for the ${}^6\Sigma$ states, using an active space with two Rydberg orbitals,

$$\sigma_{\text{CH}}, \sigma_{\text{NH}}, \sigma_{\text{NH}}^*, \sigma_{\text{CH}}^*, \sigma_{\text{Ryd}}(1), \sigma_{\text{Ryd}}(2),$$

and averaging over the first two states. This calculation provides the six sigma orbitals that correspond to the four valence orbitals $\sigma_{\text{CH}}, \sigma_{\text{NH}}, \sigma_{\text{NH}}^*, \sigma_{\text{CH}}^*$, plus two Rydberg orbitals $\sigma_{\text{Ryd}}(1)$ and $\sigma_{\text{Ryd}}(2)$. However, the indeterminacy in the MCSCF wave function means that the six orbitals in the active space are mixed in an unpredictable way, and all may include both valence and Rydberg components. Using a variation of our rotation method, we rotate the six MCSCF orbitals so that the first four of them are aligned as closely as possible with the reference orbitals $\sigma_{\text{CH}}, \sigma_{\text{NH}}, \sigma_{\text{NH}}^*$ and σ_{CH}^* . This rotation ensures that the first four MCSCF orbitals have valence character and a form similar to the corresponding (rotated) natural orbitals of the ion. The last two MCSCF orbitals have predominantly Rydberg character. We performed an independent rotation of these two orbitals so that one had primarily s character, and the other primarily p character. This rotation also preserves the relative sign of the Rydberg orbitals from one geometry to another.

At this point we combine the mo's from the ${}^1\Sigma$ HCNH $^+$ CI and the ${}^6\Sigma$ HCNH MCSCF. Specifically, using the numbering in Table 2, we take orbitals 1–9 from the ${}^1\Sigma$ HCNH $^+$ calculations to represent the core and valence space, and orbitals 10–11 from the ${}^6\Sigma$ HCNH calculations for the Rydberg space. The remaining orbitals (the virtual space) come entirely from the ${}^6\Sigma$ HCNH calculations. The rotations we have performed on each set of orbitals ensures that each of the first nine ${}^6\Sigma$ HCNH MCSCF orbitals is replaced by a similar (but not identical) orbital from the ion. The chemical interpretation of each orbital is maintained. The Gram-Schmidt orthogonalization automatically performed by GAMESS ensures that an orthonormal set of orbitals is used; note that the valence and Rydberg orbitals will not be mixed since the valence orbitals are specified first.

We used the combined set of orbitals for the final CI for HCNH. The active space is

$$\pi_{\text{CN}}, \sigma_{\text{CH}}, \sigma_{\text{NH}}, \sigma_{\text{NH}}^*, \sigma_{\text{CH}}^*, \sigma_{\text{Ryd}}(1), \sigma_{\text{Ryd}}(2),$$

and we include all single and double excitations from this space. The large active space provides a wave function that includes an even-handed description of the valence and Rydberg states discussed by Talbi & Ellinger (1998). The total number of CSF's in this calculation was 1 598 948.

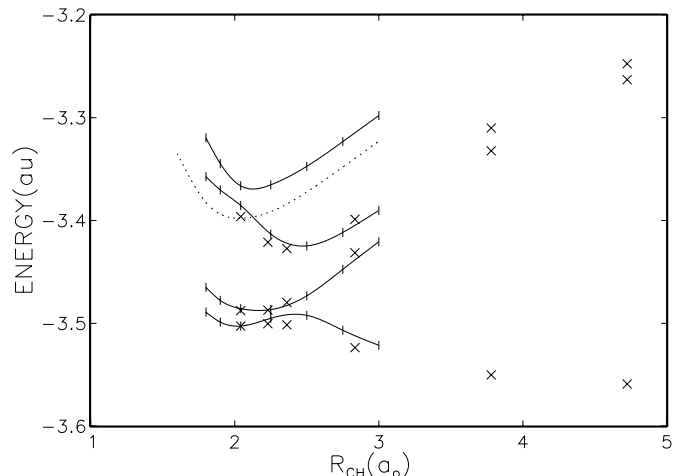


Fig. 1. The four lowest adiabatic potential curves of linear HCNH as a function of R_{CH} . The dotted line is the ion curve. The tic marks on the curves indicate the points at which calculations were performed. The solid curve is a spline. (The calculated energies have been shifted uniformly by +90 au.) The symbol (x) denotes the calculations of Talbi & Ellinger (1998), shifted vertically to agree with the present results at the ion equilibrium position.

The results of the final CI are analyzed as described in Sect. 2.1. For the way we have set up the calculation, the value of N_α is four. There were four dominant configurations in the wave functions corresponding to the first four adiabatic energies. The two corresponding to occupancies (7) and (8) make the dominant contribution to the lowest states as $R_{\text{CH}} \rightarrow \infty$ and $R_{\text{CH}} \rightarrow \infty$, respectively. Two more configurations correspond to occupancy (10), one for each of the Rydberg orbitals σ_{Ryd} . These configurations lead to diabatic Rydberg potentials parallel to the HCNH $^+$ curve. All four configurations are strongly mixed for molecular geometries close to the ion equilibrium geometry.

We also performed structure calculations for linear HCNH $^+$. For these calculations, either the R_{CH} coordinate or the R_{NH} coordinate was varied, and the others were fixed at the equilibrium values of HCNH $^+$ given in Table 1. We used the same set of orbitals and the same active space used for the final CI calculations for HCNH, and we included single and double excitations from the active space. The total number of CSF's was 734 390.

Figures 1–4 show some of the results. Figure 1 shows the adiabatic potential curves as a function of R_{CH} and the comparison with the results of Talbi & Ellinger (1998). Figure 2 shows the diagonal elements of the 4×4 $\mathbf{H}_{\text{diabatic}}$ as a function of R_{CH} . Since the most important coupling is between the Rydberg and valence configurations, we have separately diagonalized the 2×2 Rydberg block and the 2×2 dissociating block of $\mathbf{H}_{\text{diabatic}}$. Figures 3 and 4 show the corresponding results as functions of the R_{NH} . These results clearly show that there are two dissociating diabatic curves. Comparison of the CH curves and the NH curves indicates that each surface has a saddle point near the equilibrium position of the ion.

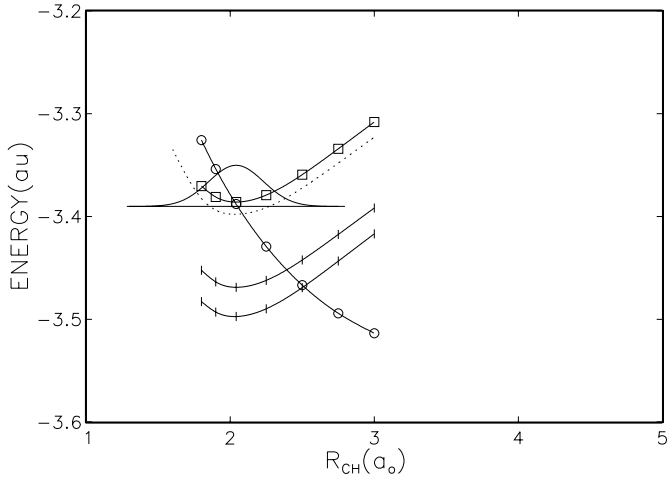


Fig. 2. The four diagonal elements of the diabatic Hamiltonian as a function of R_{CH} . The dotted line is the ion curve. (The calculated energies have been shifted uniformly by +90 au.) The $v = 0$ level of the ion and a harmonic oscillator wave function is shown (R_{CH} motion only). The symbols (O) and (□) indicate the diabatic curves dominated by the antibonding orbital σ_{CH}^* and σ_{NH}^* , respectively.

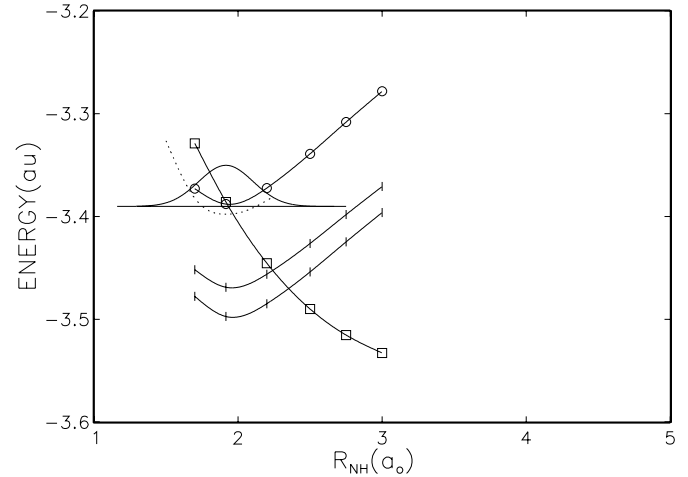


Fig. 4. The four diagonal elements of the diabatic Hamiltonian as a function of R_{NH} . The dotted line is the ion curve. (The calculated energies have been shifted uniformly by +90 au.) The $v = 0$ level of the ion and a harmonic oscillator wave function is shown (R_{NH} motion only). The symbols (O) and (□) indicate the diabatic curves dominated by the antibonding orbital σ_{CH}^* and σ_{NH}^* , respectively.

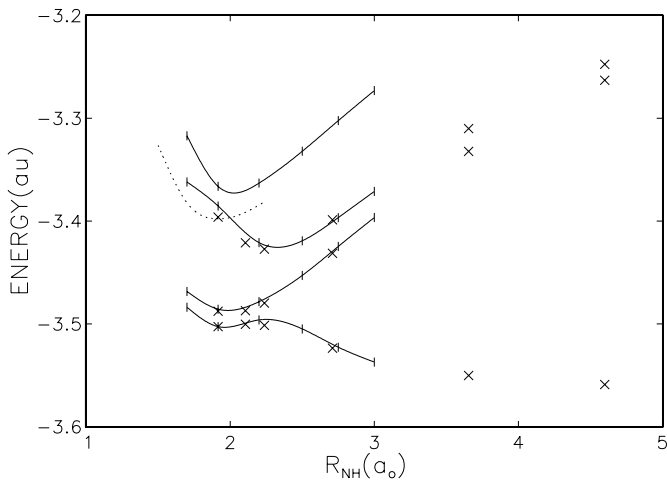
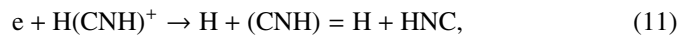


Fig. 3. The four lowest adiabatic potential curves of linear HCNH as a function of R_{NH} . The dotted line is the ion curve. The tic marks on the curves indicate the points at which calculations were performed. The solid curve is a spline. (The calculated energies have been shifted uniformly by +90 au.) The symbol (x) denotes the calculations of Talbi & Ellinger (1998), shifted vertically to agree with the present results at the ion equilibrium position.

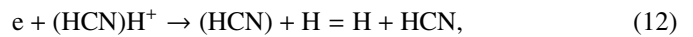
3. Dynamics calculations

The dynamics of DR has been discussed by many authors (Mitchell & Guberman 1988; Giusti-Suzor et al. 1983; Hickman 1987; Krause et al. 1992; Sarpal et al. 1994; Guberman 1997; Schneider et al. 2000; Orel et al. 2000; Larson & Orel 2001; Tennyson et al. 2003; Orel & Larson 2003; Guberman 2003). Many molecular ion targets have been considered, but the present system e + HCNH⁺ is one of the largest and most complex. Here we will implement a relatively simple approach that allows us to concentrate on the branching ratio for producing HCN and HNC. We will model each of these two channels as independent, quasi-diatomic processes.

This approach is supported by a normal mode analysis of linear HCNH⁺, which indicates very weak coupling between the in-line vibrational motions of the two hydrogens. Therefore we will calculate and compare the rates for DR for the process



and for the competing process



where the bond distances in (CNH) and (HCN) are held fixed for the purposes of each calculation.

The treatment adopted here follows the formulation of Giusti-Suzor et al. (1983) and of Hickman (1987). We consider only the direct process, but we include the nonlocal nature of the coupling terms. We solve the nuclear Schroedinger equation

$$\left(\frac{\hbar^2}{2M} \frac{d^2}{dR^2} - V^*(R) + E \right) F(R) = V_{\text{el}}(R) F(R) - i\pi V_{\text{el}}(R) \chi_0(R) \int_0^\infty \chi_0(R') V_{\text{el}}(R') F(R') dR, \quad (13)$$

where M is the reduced mass; R is the dissociating coordinate R_{CH} or R_{NH} ; $V^*(R)$ is the dissociating potential; E is the asymptotic kinetic energy of nuclear motion on $V^*(R)$, and $\chi_0(R)$ is the vibrational wave function for HCNH⁺ in R_{CH} or R_{NH} . We have assumed that the only vibrational channel open is $v = 0$, in other words, that the energy of the incident electron is below the threshold for vibrational excitation of the target HCNH⁺.

We determined $\chi_0(R)$ for the R_{CH} coordinate by fitting a few calculated points near the minimum of HCNH⁺ to a Morse potential (as a function of R_{CH} for fixed R_{NH}). A similar procedure was used to determine $\chi_0(R)$ for the R_{NH} coordinate. We then used the analytic wave functions for the Morse potential, which

can be written using Laguerre polynomials (Morse 1929). We used the reduced masses for CH and for NH, respectively.

The electronic coupling term $V_{\text{el}}(R)$ is defined as the matrix element of the electronic Hamiltonian between the incident electron wave function and the electronic resonance state that dissociates to the desired products:

$$V_{\text{el}}(R) = \langle \Psi_{e+\text{HCNH}^+} | H_{\text{el}} | \Psi_{\text{dissoc}} \rangle. \quad (14)$$

All of the necessary quantities can be directly obtained from the diabatic potential curves. $V^*(R)$ corresponds to the diagonal, dissociating elements of the diabatic Hamiltonian shown in Figs. 2 and 4. The coupling terms $V_{\text{el}}(R)$ are related to the Rydberg-valence coupling. By considering the asymptotic normalization of the continuum scattering functions that would be used to form $\Psi_{e+\text{HCNH}^+}$, and comparing the Rydberg functions that have a similar form near the molecular ion core, one finds (Talbi et al. 1989) that

$$V_{\text{el}}(R) \cong (n^*)^{1.5} \langle \Psi_{\text{Rydberg}} | H_{\text{el}} | \Psi_{\text{dissoc}} \rangle. \quad (15)$$

Here n^* is the effective quantum number of the Rydberg state; it is related to the R -dependent binding energy E_{B} of the Rydberg state relative to its parent ion by $E_{\text{B}} = 1/(2n^2)$. The matrix element on the right hand side of Eq. (15) is just the off diagonal diabatic matrix element determined by the block diagonalization. The cross section for dissociative recombination of electrons of energy ϵ is

$$\sigma(\epsilon) = \frac{\pi^2}{\epsilon} \frac{\lambda \hbar k}{2M} \lim_{R \rightarrow \infty} |F(R)|^2 \quad (16)$$

where λ is the ratio of the spin degeneracy of the dissociative state to that of the initial ion state and has the value $\lambda = 2$ in the present case. The factor $\hbar k/M$ is the asymptotic relative velocity of the dissociating fragments.

The general solution to Eq. (13) includes the possibility that the electron is captured and then re-emitted before the neutral products can be formed by dissociation. Re-emission corresponds to a ‘‘survival probability’’ of less than 1.00. In the limit that the survival probability is 1.00, Eq. (16) reduces to the simpler form

$$\sigma(\epsilon) = \frac{\pi^2}{\epsilon} \frac{\lambda \hbar k}{2M} |\langle \chi_0(R) | V_{\text{el}}(R) | F_0(R) \rangle|^2, \quad (17)$$

where $F_0(R)$ is the solution to Eq. (13) with the right hand side set equal to zero. [The asymptotic behavior of $F_0(R)$ must be normalized to $(2M/k) \sin(kR + \delta)$, where δ is the phase shift.] Equation (17) clearly shows that the DR cross section depends on the matrix element of the electronic coupling between the initial vibrational state and the final scattering state.

For the $e + \text{HCNH}^+$ reaction at low electron energies, the values of ϵ are much smaller than the asymptotic nuclear kinetic energy E , and hence the energy dependence of the cross section for direct DR is dominated by the $1/\epsilon$ factor in Eqs. (16) or (17). In this case $\epsilon\sigma(\epsilon)$ is nearly a constant, and the rate constant for DR may be well approximated by

$$\alpha(T) = \alpha(300)(300/T)^{0.5}. \quad (18)$$

We have evaluated both Eqs. (16) and (17) numerically, using values appropriate either to the CH bond or the NH bond.

We approximated V_{el} by its value at the equilibrium bond length R_{CH} or R_{NH} . In general, the results based on the simpler model Eq. (17) appears to be more realistic. The results based on Eq. (16) were much smaller, indicating a very small survival probability, and were not consistent with recent laboratory experiments. It is possible that vibrational modes of HCNH that are not linear (such as bending) play an important role in stabilizing the neutral molecule by causing transitions to electronic states not strongly coupled to the electron continuum. We also note that our handling of the survival probability is consistent with the approximation of Tachikawa (1999).

Our numerical results confirm that $\epsilon\sigma(\epsilon)$ is nearly constant; the precise values we obtained were 2.93 eV \AA^2 for dissociation of the R_{CH} bond and 2.84 eV \AA^2 for the R_{NH} bond. These values correspond to $\alpha(300) = 1.22 \times 10^{-7} \text{ cm}^3/\text{s}$ (for the CH bond breaking) and $\alpha(300) = 1.18 \times 10^{-7} \text{ cm}^3/\text{s}$ (for the NH bond breaking). Taking into account all the uncertainties in our calculation, we conclude that our model yields similar values of order $1 \times 10^{-7} \text{ cm}^3/\text{s}$ for each DR channel. For comparison, Semaniak et al. (2001) obtained $\alpha(T) = 2.8 \times 10^{-7} \text{ cm}^3/\text{s} (300/T)^{0.65}$, and Adams & Smith (1988) measured $3.5 \times 10^{-7} \text{ cm}^3/\text{s}$ at $T = 300$ K. These measurements are summed over all final states of DR, including channels not included in our simple model.

Our major conclusion is that for the potential curves and couplings we determine, the direct mechanism is effective and can account for a substantial part of the large rate constants observed. We see no evidence that the rates for formation of HCN and HNC should be substantially different. Although the indirect mechanism may play a role as well, we have not attempted to include this mechanism. Any treatment of the indirect mechanism within the framework of our linear model would be rather crude; other work Tachikawa (1999) has found that bending motion plays a strong role in the indirect process.

4. Concluding remarks

We have performed electronic structure calculations for neutral HCNH and the molecular ion HCNH^+ , including a diabaticization using the block diagonalization method. The results confirm the earlier calculations of Talbi & Ellinger (1998), who concluded that the dissociating curves cross the ionic curves near the equilibrium position. We have also investigated the relative rates for dissociative recombination (DR) leading to the final channels $\text{H} + \text{HNC}$ and $\text{H} + \text{HCN}$. Implementing the direct mechanism of DR and a simple quasi-diatomic model, we find similar rates (of order $1 \times 10^{-7} \text{ cm}^3/\text{s}$) for the production of HNC and HCN. Further investigation of this difficult problem is needed for a definitive treatment of all the vibrational modes as well as direct and indirect processes.

Acknowledgements. A.P.H. was supported by NSF Grant No. PHY-0244767. R.D.M. was supported by the USDE GAANN program. C.H. was supported by the REU site grant at the Department of Physics at Lehigh University. DT was supported by CNRS program PN-PCMI.

References

- Adams, N. G., & Smith, D. 1988, *Chem. Phys. Lett.*, 144, 11
- Bardsley, J. N. 1968, *J. Phys. B*, 1, 349
- Carlson, B. C., & Keller, J. M. 1957, *Phys. Rev.*, 105, 102
- Dunning, Jr., T. H., & Hay, P. J. 1977, *Methods of Electronic Structure Theory*, ed. H. F. Shaeffer, III (New York: Plenum Press), 1
- Edmiston, C., & Ruedenberg, K. 1963, *Rev. Mod. Phys.*, 35, 457
- Giusti, A. 1980, *J. Phys. B*, 13, 3867
- Giusti-Suzor, A., Bardsley, J. N., & Derkits, C. 1983, *Phys. Rev. A*, 28, 682
- Guberman, S. L. 1997, *Science*, 278, 1276
- Guberman, S. L. (ed.) 2003, *Dissociative Recombination of Molecular Ions with Electrons* (New York: Kluwer Academic/Plenum Publishers)
- Hickman, A. P. 1987, *J. Phys. B*, 20, 2091
- Irvine, W. M., & Schloerb, F. P. 1984, *ApJ*, 282, 516
- Krause, J. L., Orel, A. E., Lengsfeld, III, B. H., & Kulander, K. C. 1992, in *Time Dependent Quantum Molecular Dynamics: Experiments and Theory*, ed. J. Broeckhove, & L. Lathouwers (New York: Plenum Press), 131
- Larson, Å., & Orel, A. E. 2001, *Phys. Rev. A*, 64, 062701
- Mitchell, J. B. A., & Guberman, S. L. (ed.) 1988, *Dissociative Recombination: Theory, Experiment, and Applications* (New York: World Scientific)
- Morse, P. M. 1929, *Phys. Rev.*, 34, 57
- Orel, A. E., & Larson, Å. 2003, in *Dissociative Recombination of Molecular Ions with Electrons*, ed. S. L. Guberman (New York: Kluwer Academic/Plenum Publishers), 1
- Orel, A. E., Schneider, I. F., & Suzor-Weiner, A. 2000, *Phil. Trans. R. Soc. Lond.*, 358, 2445
- Pacher, T., Cederbaum, L. S., & Köppel, H. 1988, *J. Chem. Phys.*, 89, 7367
- Roos, B. O. 1987, *Adv. Chem. Phys.*, 69, 399
- Sarpal, B. K., Tennyson, J., & Morgan, L. A. 1994, *J. Phys. B*, 27, 5943
- Schilke, P., Walmsley, C. M., Pineau des Forêts, G., et al. 1992, *A&A*, 256, 595
- Schmidt, M. W., Baldrige, K. K., Boatz, J. A., et al. 1993, *J. Comp. Chem.*, 14, 1347
- Schmidt, M. W., & Gordon, M. S. 1998, *Ann. Rev. Phys. Chem.*, 49, 233
- Schneider, I. F., Rabadán, I., Carata, L., et al. 2000, *J. Phys. B*, 33, 4849
- Semaniak, J., Minaev, B. F., Derkatch, A. M., et al. 2001, *ApJS*, 135, 275
- Shiba, Y., Hirano, T., Nagashima, U., & Ishii, K. 1998, *J. Chem. Phys.*, 108, 698
- Spirko, J. A., Mallis, J. T., & Hickman, A. P. 2000, *J. Phys. B*, 33, 2395
- Szabo, A., & Ostlund, N. S. 1982, *Modern Quantum Chemistry: Introduction to Advanced Electronic Structure Theory* (New York: Macmillan Publishing Co., Inc.)
- Tachikawa, H. 1999, *Phys. Chem. Chem. Phys.*, 1, 4925
- Talbi, D., & Ellinger, Y. 1998, *Chem. Phys. Lett.*, 288, 155
- Talbi, D., Hickman, A. P., Pauzat, F., Ellinger, Y., & Berthier, G. 1989, *ApJ*, 339, 231
- Talbi, D., Pauzat, F., & Ellinger, Y. 1988, *Chem. Phys.*, 126, 291
- Tennyson, J., Gorfinkiel, J. D., Rozum, I., Trevisan, C. S., & Vinci, N. 2003, *Radiat. Phys. Chem.*, 68, 65